Theo DuBose Thesis

Theo DuBose

April 24, 2012

Part I

Immunospecific Gold Nanoparticles for Contrast Enhancement of Corneal Tissue Culture

1 Introduction

According to the National Eye Institute (NEI), approximately 40,000 cornea transplants are performed every year in the United States. Unfortunately, about 20 percent (8000 per year) of these transplants are rejected [5], necessitating a second transplant. An increase in the number of procedures is inconvenient for the patient at best; therefore, it is desirable to find ways to minimize the amount of rejection as well as increase the overall supply of tissue for cornea transplants.

1.1 Corneal Engineering

Prof. Liz Orwin's lab at Harvey Mudd College is attempting to overcome the challenges of cornea transplants by growing replacement corneas. This is done by electrospinning collagen fibers, then seeding cells from a patient who needs new corneas. However, the electrospun collagen does not possess the structural properties of corneal collagen, so the Orwin Lab is focused on finding ways to control the phenotype and regulatory mechanisms of the cells. It is hoped that through this process, the cells will reenact the initial formation of the corneas in fetal development, taking up the electrospun collagen and laying it back down in the native form, viz., a hexagonal close-packed array of 30 nm-diameter collagen fibrils.

In order to better understand the behavior of the cells in response to the treatments they receive, Prof. Orwin's lab would like to be able to monitor both the position and phenotype of the cells in the scaffold. Confocal microscopy, a standard biological imaging modality, has a high ($< 1\,\mu$m isotropic) resolution but can only image 25 μm deep. The high resolution makes confocal desirable, but human corneas are 500 μm thick, and the collagen scaffolds can be thicker, making confocal unusable for full 3D imaging. In contrast, the optical coherence microscope (OCM) trades high resolution for moderate resolution ($5\,\mu$m lateral, $10\,\mu$m axial) and over 1 mm of depth penetration at 850 nm wavelength. Consequently, the OCM was employed to monitor the cells.

Unfortunately, the collagen in the scaffold scatters too highly for the OCM to distinguish the cells, so Chris Raub '04 proposed a method, developed from a paper by Sokolov [11], wherein 35 nm gold nanoparticles would be applied to increase scattering of the cells via a process called indirect immunolabeling, the basic precepts of which are still used in this project [10]. Indirect immunolabeling has four key components: a target protein (we are targeting $\alpha 5\beta 1$-integrin), a primary antibody that is *anti-* the target protein, a secondary antibody that is *anti-* the primary antibody, and a label (both the gold nanoparticles and a fluorescent molecule on the secondary antibody). Indirect immunolabeling is implemented by first binding primary antibodies. Then, secondary antibodies (anti-Ab1) are bound to nanoparticles via van der Waals forces. The antibody-gold is then allowed to bind to the Ab1-protein-cell *in vitro*. A schematic diagram of this process is shown in Figure 1.

Jamie Shoffeit '05 [1], Megan Arman '06, and Emily Hogan '07 all followed on Raub's work to achieve labeling. The process they consisted of creating 35 nm diameter gold nanoparticles from a citrate reduction of Au(III) and binding the antibodies to the nanoparticles via van der Waals forces alone. Although Hogan was finally able to use this technique to produce a statistically significant increase in scattering in 2007, the scattering increase was not as great as was desired.

To address this, David Coats '08 did a number of studies to optimize the gold being used as the labeling agent. Coats performed extensive calculations using Mie theory to maximize scattering. Mie theory details the scattering pattern of particles on the order of

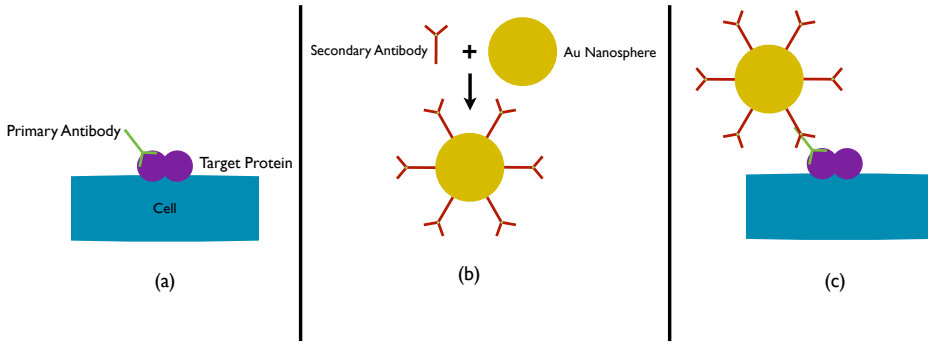

Figure 1: Stages of indirect immunolabeling presented schematically (not to scale). (a) The primary antibody, MAB199, binds to the targeted surface protein, $\alpha 5\beta 1$-integrin. (b) Secondary antibodies, AP124F, are bound to the surface of a gold nanoparticle. (c) A gold nanoparticle-secondary antibody complex binds to the primary antibody, which is in turn bound to the surface protein.

or larger than the wavelength of light they scatter. As even a 35 nm nanoparticle cannot be approximated as a point when using 850 nm light, Mie theory provides a far more accurate prediction of the intensity of backscattered intensity than Rayleigh scattering theory. These calculations showed that for any diameter, a particle made of solid gold (versus a particle with an inner core of silica) gave the highest scattering to absorption cross-section ratio, as shown in Figure 2. As can also be seen in that image, C_{sca}/C_{abs} also increases with diameter, up to a point. However, the settling rate of the gold particles also had to be taken into account, as well as the availability of manufactured gold nanoparticles. With these multiple factors in consideration, it was decided that 90 nm diameter nanoparticles from Nanopartz would be used. With these improved gold particles, David Coats again performed imaging tests on a monolayer of cells. However, the same lack of obvious signal generation prompted even further investigation.

One concern regarding the labeling system was that the antibodies were bound to the gold with only van der Waals forces. Rob Warren '10 [13] discovered a procedure in a paper by Lowery et al. [7] by which increased binding had been achieved for immunolabeling. The procedure is called PEGylation because of its use of polyethylene glycol polymer chains; a schematic diagram of the process is shown in Figure 3. The procedure consists of using a polyethylene glycol (PEG) polymer chain functionalized at one end with orthopyridyl disulfide (OPSS) and at the other with an N-Hydroxysuccinimide ester (NHS). The OPSS-PEG-NHS is incubated with the antibody for 24 hours, in which time the NHS ester reacts with a lysine in the antibody, leaving the NHS ester free in solution and the antibody attached to the OPSS-PEG. This OPAb, as we call it, is then incubated with the gold for 24 hours, so that the OPSS group splits at the disulfide bond and the PEG chain attaches to the gold via a thiol bond, which has a strength slightly less than that of a covalent bond and much larger than that of a van der Waals bond !(appendix or footnote or reference on thiol bonds?). This should ensure that the antibody is firmly attached to the gold. The second part of the procedure is to prevent any other molecules from binding with the gold. This is accomplished by binding another PEG chain to the gold, of which one end is functionalized

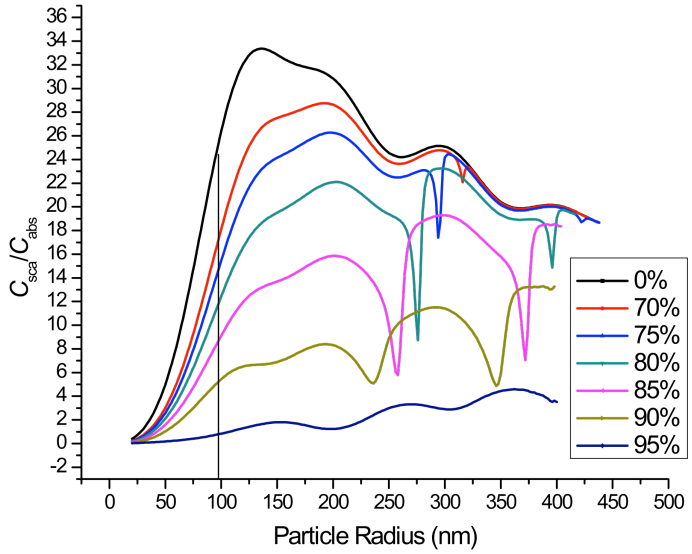

Figure 2: Plot of the ratio of the scattering cross section C_{sca} to the absorption cross section C_{abs} as a function of total particle diameter, calculated via Mie theory. Line color, as indicated by legend, corresponds to percent of total diameter taken up by silica inner core. Index of refraction values used are $n_{\text{Au}} = 0.194 - 5.527i$, $n_{\text{silica}} = 1.44$, and $n_{\text{water}} = 1.33$ for the surrounding region. From [2].

with a thiol group (SH) that then forms a thiol bond with the gold. This should fill on any space left after the addition of the OPAb.

Unfortunately, these tests also failed to produce the desired specific increase in scattering, so in Summer 2010 Oliver Hoidn and Perry Ellis '11 undertook a reexamination of the PEGylation protocol. Several significant results emerged from their studies that indicated problems with the PEGylation protocol. First, the gold, though its pH is advertised as between 6 and 8, was actually measured at a pH between 5 and 5.5 [3] due to the lack of a buffer in the solution. However, if commercial PBS is added, the salt in that solution screens the negative capping agent on the gold nanoparticles, thus eliminating the mutual repulsion between the nanoparticles and causing them to agglomerate and fall out of solution. To remedy this, a buffer solution made of $Na_2HPO_4{\cdot}7H_2O$ and $NaH_2PO_4{\cdot}H_2O$ was added to the gold to achieve a total salt concentration of 10 mM. This concentration was chosen as it provides a sufficient level of buffering without screening the capping agent too much. However, over the course of the several days required for the PEGylation process, it was found that the gold still suffered from a high rate of agglomeration. A footnote was then found in Lowery et al. [7] that noted that PEG-SH cannot perform its protective function unless it has a molecular weight of at least 5 kDa. As the PEG-SH used up to that point had been of molecular weight 1.2 kDa, it had not protected the gold.

Thus, after Oliver and Perry concluded their work, it remained to readjust the PEGylation protocol for 5 kDa PEG-SH, and to use that updated protocol to demonstrate a statistically significant contrast increase. In addition, it was discovered that the NHS ester used to

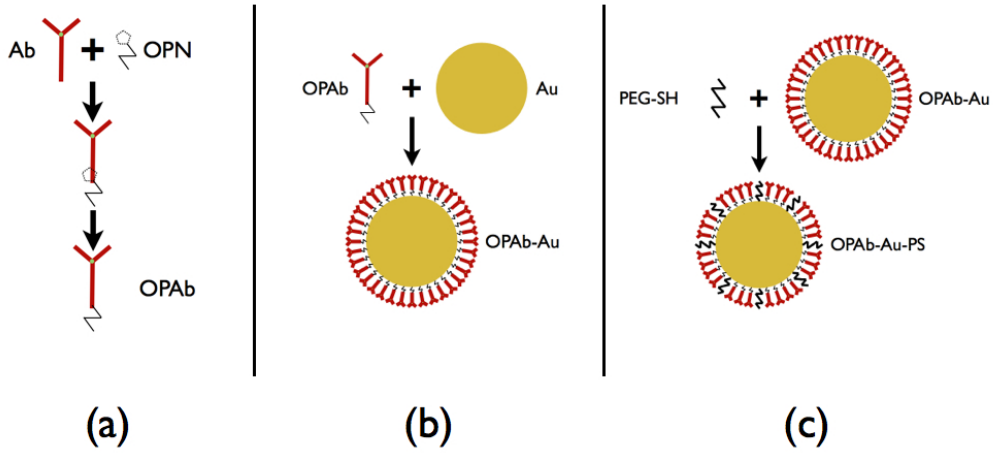

Figure 3: Schematic diagram of the PEGylation process. (a) The OPSS-PEG-NHS (OPN) binds to the antibody (Ab) to form OPAb. (b) The OPAb binds to the Au nanosphere to form OPAb-Au. (c) The PEG-SH fills in the gaps on the surface of the OPAb-Au, forming OPAb-Au-PS and protecting the sphere.

bind the OPN to the antibody can undergo hydrolysis, rendering it incapable of binding; therefore, it was also necessary to examine the hydrolysis of the NHS ester. To date, the issue of NHS hydrolysis has been settled (Ch.chapter 2) and the PEGylation protocol has been optimized with the 5 kDa PEG-SH (Ch.chapter 3). The optimized protocol produces results consistent with the model of PEGylation we have developed (Ch.chapter 4). In addition, the 5 kDa PEG-SH appears to provide excellent long-term protection to the spheres. Spheres made with the optimized protocol have been used in two labeling experiments (Ch.chapter 5 andchapter 6), which have provided further insights into the immunolabeling process.

2 Addition of Antibodies to Nanospheres

At the end of Summer 2010, Oliver Hoidn and Perry Ellis had determined that the optimal number of OPSS-PEG-antibody (OPAb) molecules per nanosphere was approximately 2000; however, there were significant concerns as to whether the OPSS-PEG-NHS (OPN) was successfully binding to the lysines on the antibody, or whether monolayer formation was simply the result of the antibodies binding to the nanospheres via van der Waals forces. The OPN reaction occurs by substituting the NHS ester for a primary amine, such as the one found on the functional groups of lysines in an antibody. A diagram of this reaction is shown in Figure 4.

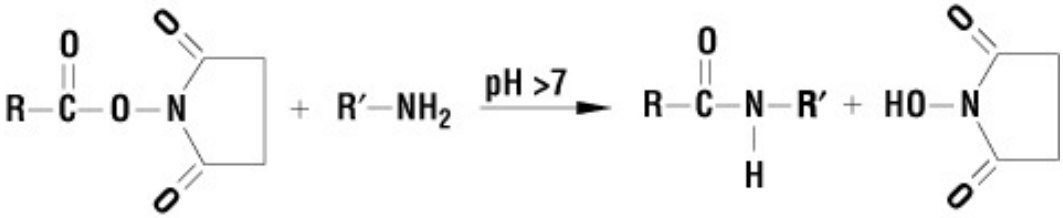

Figure 4: Schematic diagram of the OPN+antibody→OPAb reaction. **R** represents the OPSS-PEG, and **R'** represents the antibody. The reaction is favored in basic conditions. From [9]

OPN comes in a lyophilized form, and the reaction with the antibody does not occur until the OPN is in solution. However, once the OPB is in solution, a competing reaction begins in which hydrolysis occurs and the NHS ester is replaced with a hydroxyl group instead of an amine. This renders the molecule unable to bind to antibodies, and the half-life of the hydrolysis reaction can be on the order of minutes at pH 8 [6]. Consequently, there was a concern that a large portion of the OPN used in the OPN+antibody→OPAb reaction was not binding to the antibody.

Fortunately, a direct physical measurement can be used to quantify the hydrolysis of the NHS ester. The free NHS ester in solution absorbs at 260 nm much more strongly than the bound ester [8]. Therefore, the Cary 5000 UV-Vis-IR Spectrophotometer was used to monitor the absorption at 260 nm over the course of several hours. The results of this measurement are shown in Figure 5.

Based on the coefficient of the exponent, $C_3 = 0.00523\,\mathrm{min}^{-1}$, we can calculate that the half-life of NHS ester hydrolysis at pH 7.5 is

$$\tau_{1/2} = \frac{\ln 2}{C_3} = 133\,\mathrm{min}$$

or about two hours.

Two conclusions can be drawn from this: first, there is very little danger of having no bound NHS remaining when the protein is added, since that should occur at the most 10 minutes after the OPN solution is created (and will most likely be less than five minutes after solution creation). Second, this confirms the need to incubate the protein with the OPN overnight. Since both hydrolysis of the NHS and the reaction with the lysine work on a similar mechanism, their rates can be expected to be comparable. Thus, in order to create as much OPAb as possible, at least four hydrolysis half-lives are necessary to achieve $> 90\%$ yield. However, since the hydrolysis is nontrivial on that time scale, OPN should

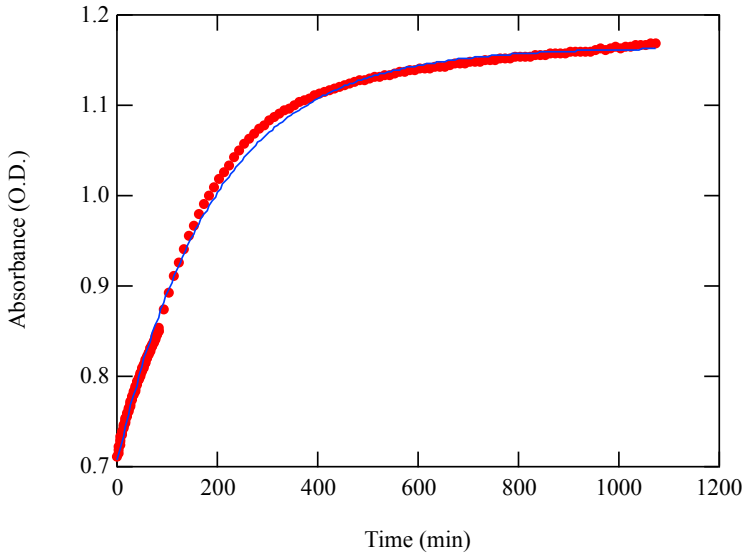

Figure 5: Plot of the absorbance of the OPN solution over time. The reaction rate seems to be proportional to concentration, giving a simple first-order rate law. The lower density of points at ∼80 minutes occurred because the spectrophotometer was set to record a spectrum every 10 minutes rather than every 1 minute. The blue line displays a fit to $A = C_1 + C_2\, e^{-C_3 t}$. The fitted values were $C_1 = 1.16$, $C_2 = -0.458$, and $C_3 = 0.0052$

be used in a factor of 2 excess in order to facilitate maximal protein binding. Therefore, in the PEGylation procedure, we will use 2,000 antibodies per Au nanosphere and 4,000 OPN molecules per nanosphere (see **??**).

3 Addition of PEG-SH to Nanospheres

With the questions about OPN-to-antibody and OPAb-to-nanosphere binding settled, it still remained to determine the optimal concentration of PEG-SH (PS). The PEG-SH is used expressly for the purpose of protecting the gold nanospheres from agglomerating when placed in a salt solution, e.g. the phosphate-buffered saline (PBS) solution present in a cell culture. However, Ellis and Hoidn found that the 1 kDa PEG-SH used since PEGylation was first introduced [13] failed to adequately protect the spheres, leading to a significant degree of agglomeration, as shown in Figure 6. A footnote found by Ellis and Hoidn in Lowery et al. [7] noted that PEG-SH with a molecular weight less than 5 kDa does not protect gold, explaining the failure of the 1.2 kDa PEG-SH.

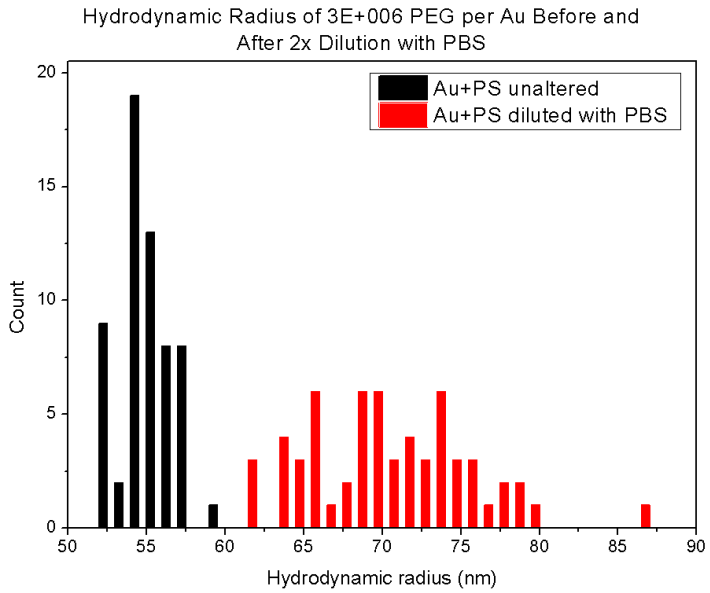

Figure 6: Histogram of radii of acquisitions of 3×10^6 1 kDa PS/Au with and without PBS from Summer 2010. The distribution is noticeably shifted to the right and flattened after the addition of PBS. Data taken by Ellis and Hoidn [3].

At the end of Summer 2010, 5 kDa PEG-SH had not yet been used or characterized, so a completely new optimization process had to be a applied. This consisted of measuring the radii of the gold spheres immediately after the addition of a variety of concentrations of 5 kDa PEG-SH (section 3.1); measuring the radii of the same solutions after an incubation period (section 3.2); and measuring the radii of some solutions after addition of salt solution (section 3.3). These measurements yielded a monolayer number for 5 kDa PEG-SH of approximately 50,000 PS/Au. Strong protection of the nanospheres was also demonstrated at 10,000 PS/Au. Therefore, 10,000 PS/Au was used as the concentration for the full protocol, as it provides protection, and there should already be a monolayer of OPAb on the surface of the nanospheres.

3.1 Titration Study

A titration curve was made by adding 5 kDa PS to 90 nm gold nanospheres (R=52 nm) in varying concentrations, from 1000 PS per nanosphere to 10^7 PS per nanosphere; the broad range was used to determine the range of concentrations in which the monolayer formed. The hydrodynamic radii of these PEGylated nanospheres were then measured using the Dynamic Light Scattering (DLS) instrument, taking 15 30-second acquisitions of each solution and discarding the first three to account for temperature acclimation. The results of these exploratory measurements are shown in Figure 7.

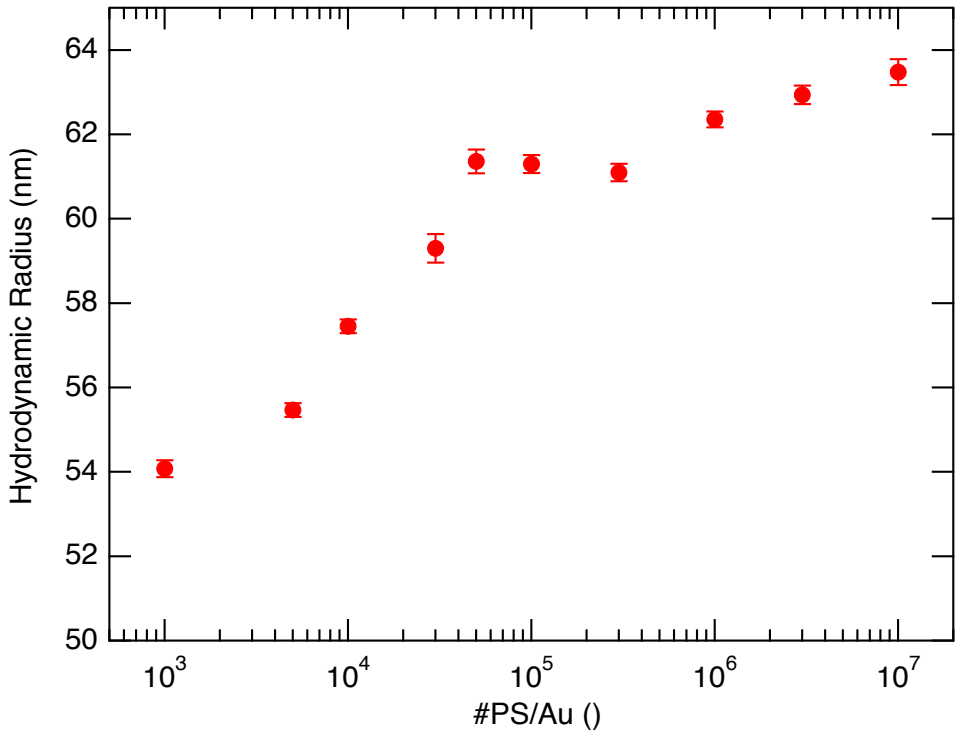

Figure 7: Plot of hydrodynamic radii of Au nanospheres from 1,000 to 10^7 PS/Au less than 30 minutes after addition of PS.

This plot shows the behavior of a rapid rise followed by a plateau that is expected of a species forming a monolayer on a surface. The plateau begins to appear around 100,000 #PS/Au, so two more measurements were taken with a spread of concentrations around that range. A plot of the averages of the radii of the repeated concentrations are shown in Figure 8. This data suggests that the monolayer is formed at approximately 50,000 #PS/Au, with a radius of 60.4 ± 0.3 nm.

3.2 Time Study

The same samples used in the titration study were measured again after 48–72 hours of incubation, producing the radii shown in Figure 9.

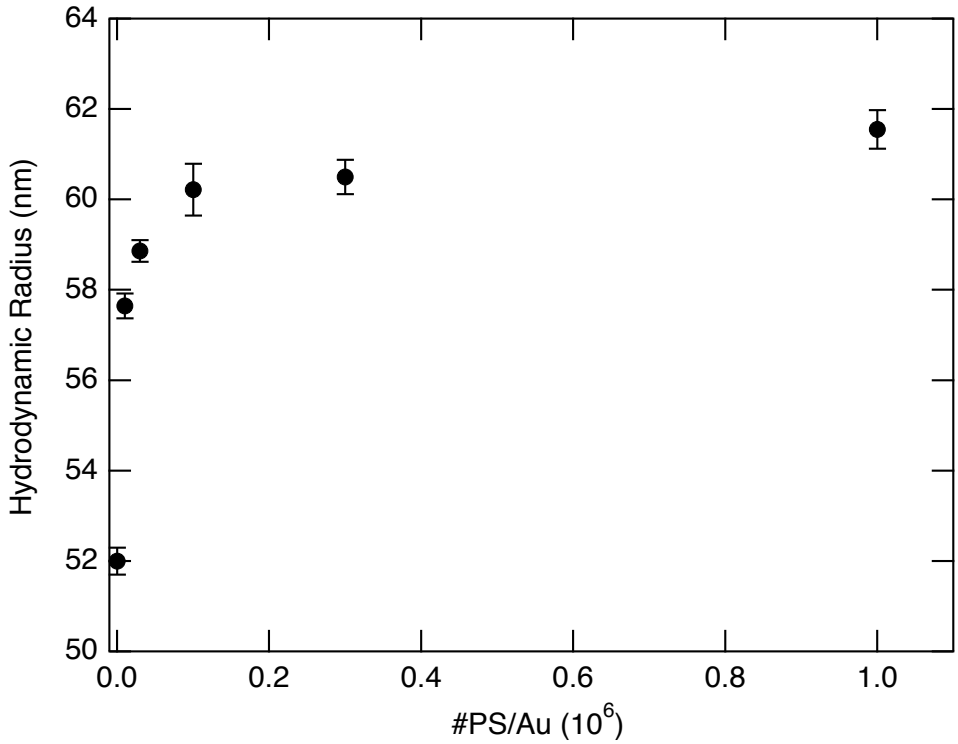

Figure 8: Plot of hydrodynamic radii of Au nanospheres at 10,000, 30,000, 100,000, 300,000, and 10^6 PS/Au less than 30 minutes after addition of PS. Points are formed by taking the mean and standard error of three independent measurements at each concentration.

The plateau in this graph is much sharper than in Figure 8, indicating that van der Waals forces and thiol bonding processes are in competition, with van der Waals binding dominating immediately after addition, but the lower-energy thiol bonds dominating after incubation time. This leads to the increased radius of the lower-radius samples and the decreased radius of the higher-radius samples. However, the plateau region still has $R = 60.3 \pm 0.3$ nm, as a second indication of a monolayer. Clearly, it is essential that PEG-SH be allowed to incubate with spheres to allow for the PEG-SH binding to reach equilibrium.

More information about the final monolayer state can be gained from determining the apparent number of PEG-SH molecules bound to the nanosphere. A single 5 kDa PEG-SH molecule, with a density of $1.11\,\frac{\mathrm{g}}{\mathrm{cm}^3}$, has a volume of

$$\mathrm{V}_{5\,\mathrm{kDa\ PEG-SH}} = \frac{5\mathrm{kDa}}{1.11\frac{\mathrm{g}}{cm^3}} = 7.5\,\mathrm{nm}^3$$

This means that a 5 kDa PEG-SH monolayer has, based on the change in hydrodynamic radius,

$$\#_{5\,\mathrm{kDa\ PEG-SH}} = \frac{\frac{4}{3}\pi((60.5\,\mathrm{nm})^3 - (51.5\,\mathrm{nm})^3)}{V_{5\,\mathrm{kDa\ PEG-SH}}} = 47,500\ 5\,\mathrm{kDa\ PEG-SH}$$

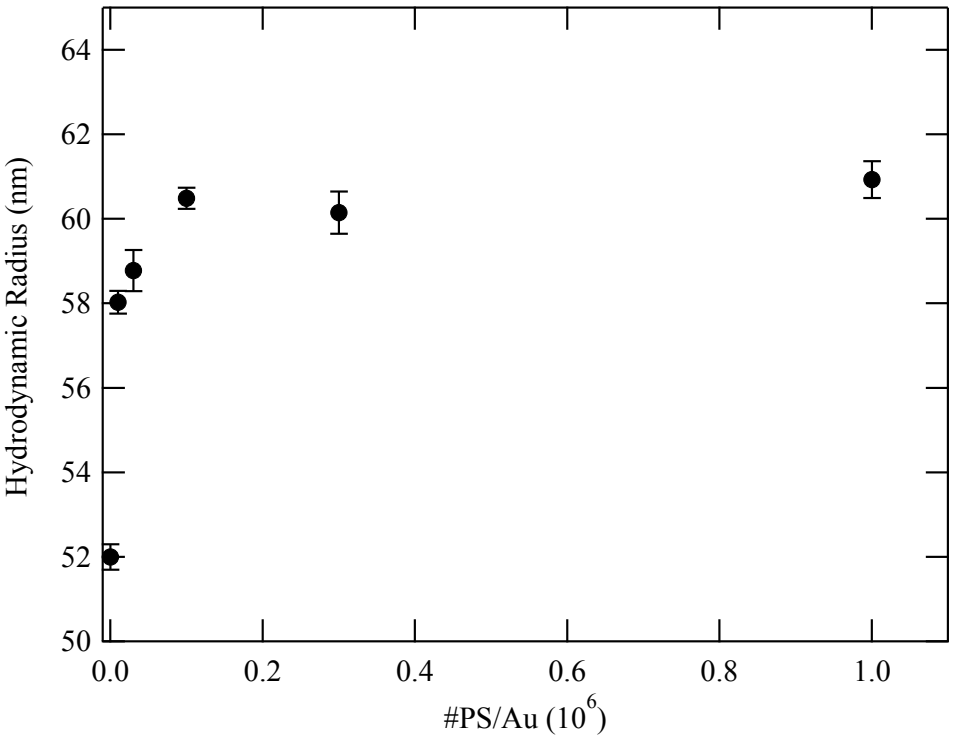

Figure 9: Plot of hydrodynamic radius of Au nanospheres at the same concentrations as in Figure 8 48–72 hours after addition of PS. Points are formed by taking the mean and standard error of three independent measurements at each concentration.

This indicates that the measurement of the plateau as beginning at 50,000 PEG-SH per nanosphere is correct. This also allows us to get a sense of the effective footprint of a PEG-SH molecule as it sits on the gold. At monolayer concentration, the area on the surface of the gold taken up by each PEG-SH molecules is

$$A_{\mathrm{PS}} = \frac{4\pi(51.5\,\mathrm{nm})^2/\mathrm{Au}}{47,500\,\frac{\mathrm{PS}}{\mathrm{Au}}} = 0.70\frac{\mathrm{nm}^2}{\mathrm{PS}} = 70\frac{^2}{\mathrm{PS}}$$

This size is determined partially by the atomic size of the sulfur atom ($D = 2\mathrm{A}$), but mostly by the extent to which the PEG chain is bunched; clearly, most of the effective width comes from the bunching.

3.3 Protection Study

As mentioned above, the main reason for using 5 kDa PEG-SH is to prevent the Au nanospheres from agglomerating. The Au nanosphere solution includes a negatively charged capping agent that makes the spheres repel each other; when the solution is buffered at pH $\sim$7.5 to prevent antibodies from denaturing during the full immunogold procedure, positive

ions are introduced into the solution that neutralize the capping agents, causing the gold nanospheres to agglomerate. Theoretically, PEG-SH would prevent this from happening, but 1 kDa PEG-SH does not, as shown in Figure 6.

Therefore, the protection capabilities of 5 kDa PS were tested by adding PEG-SH to the Au nanospheres in various concentrations, then mixing those solutions in equal volumes with commercial PBS, which has a salt concentration over 100 mM!!. The spheres were allowed to incubate for at least 30 minutes with the PBS, then measured in the DLS. Selected results from those measurements are shown in Figure 10.

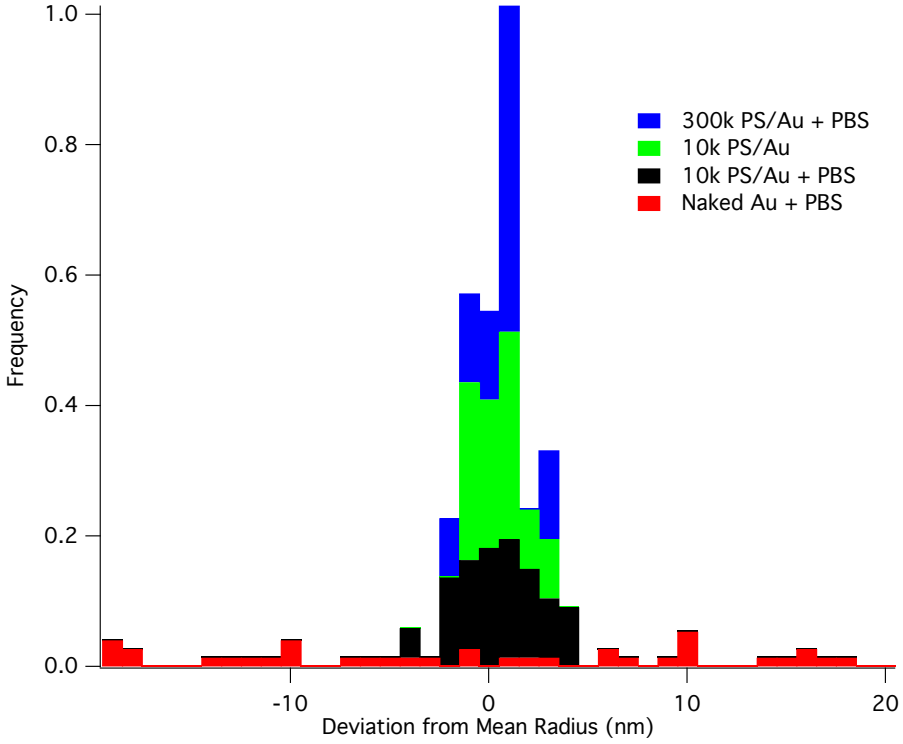

Figure 10: Stacked histograms of differing concentrations of Au-PS with and without PBS. The naked gold is significantly broader than any of the other distributions.

For all but the naked gold, almost all acquisitions are within 3 nm of the mean; this is also true of the 300k PS/Au without PBS from Summer 2010. However, with just 10k 5 kDa PS/Au, the width of the distribution barely widens when PBS is added–a stark contrast to the addition of PBS to 300k 1 kDa PS/Au. Furthermore, there was a $\sim$15 nm increase in average radius between the 1 kDa PS spheres with and without PBS. In the case of the 10k 5 kDa PS/Au, the difference in average radius was negligible: 0.09 nm.

From observing the lack of change in both average radius and the change in radial distribution when using the 5 kDa PEG-SH, it is clear that the 5 kDa PEG-SH fully protects the Au nanospheres against capping agent neutralization. There is, however, a noticeable difference between the 10k and 300k PS/Au samples; the 300k is slightly narrower, indicating that it offers slightly more protection, consistent with the 300k PS/Au solution being on the plateau while the 10k PS/Au is still on the rising part of the titration curve.

4 Results of the Full Protocol

Several fully labeled and protected nanosphere samples were created during the '11–'12 year. The protocol used was adapted from Oliver Hoidn and Perry Ellis's report [3], using 2,000 antibodies per Au nanosphere and the curve-elbow value 10,000 PEG-SH molecules per Au nanosphere. Detailed documentation of the protocol can be found in **??**.

The progress of the protocol was monitored by a DLS radius measurement at five or six stages:

1. Immediately after the addition of the OPAb
2. 24 hours after the addition of the OPAb
3. Immediately after the addition of the PEG-SH
4. 24 hours after the addition of the PEG-SH
5. After dilution with equal parts PBS, to check for protection
6. (For most but not all samples) 48 hours after the addition of PEG-SH

The results of these measurements are shown in Figure 11. The data shows an immediate increase of 6–8 nm upon the addition of the OPAb, followed by slight (<0.1 nm) gains after 24 hours of incubation. AP124F is an IgG antibody and has dimensions of approximately $14.5\,\text{nm} \times 8.5\,\text{nm} \times 4.0\,\text{nm}$ [12] as shown in Figure 12; since the NHS replacement can occur on any lysine or N terminus (of which there are several), a 6–8 nm increase in radius is reasonable when all spatial orientations are taken into account.

Additional analysis can be performed by using the same number estimation as in chapter 3. An OPAb conjugate should have a volume of

$$V = V_{\text{PEG}} + V_{\text{Ab}} = \frac{2.1\text{kDa}}{1.11\frac{\text{g}}{cm^3}} + \frac{160\text{kDa}}{1.35\frac{\text{g}}{cm^3}} = 200\,\text{nm}^3$$

Examining the hydrodynamic volume change after the addition of PEG-SH, this corresponds to

$$\frac{4}{3}\pi[(58\,\text{nm})^3 - (51.5\,\text{nm})^3]/\frac{200\,\text{nm}^3}{OPAb} = 1230\ \text{OPAb}$$

However, this may be an over-estimate, as the $1.35\ \frac{\text{g}}{\text{cm}^3}$ density is for the crystalline state of protein [4]; the actual effective volume of the OPAb in solution may be larger. Further uncertainty is introduced by the complexity of the diffusion of an Au nanosphere with over 1000 OPAb molecules attached to it. Therefore, this calculation serves primarily as an order-of-magnitude check; in that sense, 1230 OPAb/Au compares quite favorably to the 2000 OPAb/Au in solution.

We can again perform a calculation of effective footprint:

$$A_{\text{OPAb}} = \frac{4\pi(51.5\,\text{nm})^2/\text{Au}}{1230\frac{\text{OPAb}}{\text{Au}}} = 27.1\,\frac{\text{nm}^2}{\text{OPAb}}$$

This is considerably larger than the effective width of the PEG-SH, indicating that the OPAb molecules on the nanosphere sterically hinder other OPAb molecules from forming thiol bonds with the nanosphere surface. Since the binding mechanism between the PEG chain and the gold surface is the same, this means that there is likely additional room for

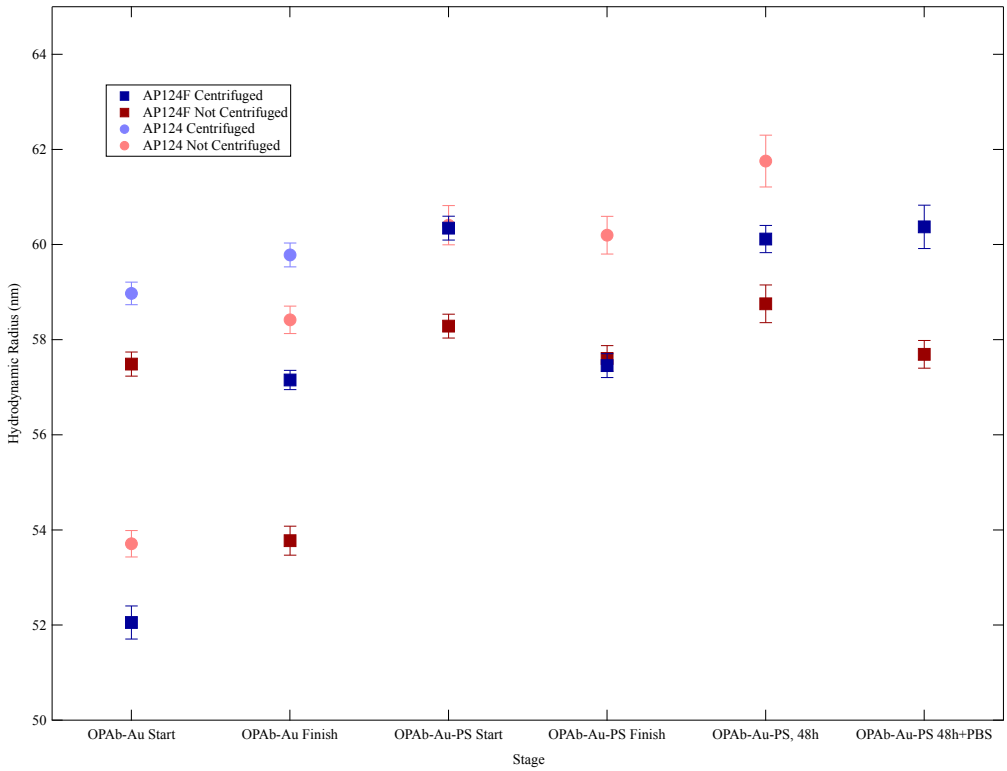

Figure 11: Plot of hydrodynamic radii of multiple solutions at each step in the protocol. NOTE: PLACEHOLDER UNTIL I COLLATE ALL THE DATA.

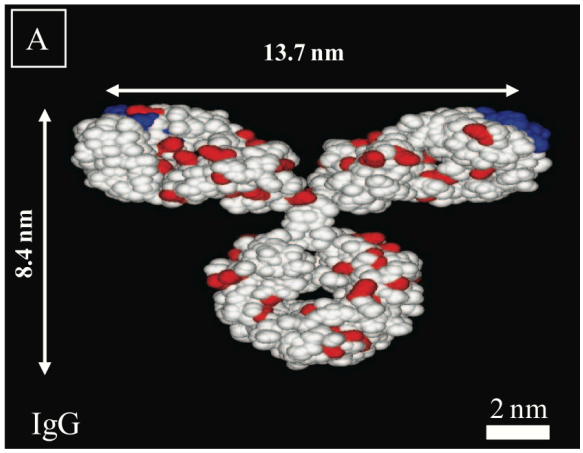

Figure 12: Structural dimensions of an IgG antibody. From [12].

thiol bonds on the surface, which means that that the PEG-SH should fill in gaps on the surface of the sphere.

Performing the same volumetric analysis on the change in radius from OPAb-Au to OPAb-Au-PS, we see that the number of PS molecules bound to the OPAb-Au is approximately

$$\frac{4}{3}\pi[(59\,\mathrm{nm})^3 - (58\,\mathrm{nm})^3]/\frac{7.5\,\mathrm{nm}^3}{PS} = 5730\ \mathrm{PS}.$$

This number is the right order of magnitude, given that 10,000 PS/Au were added, and only the gaps on the surface are expected to be filled.

The addition of PEG-SH brings the total number of thiol bonded PEG chains on the Au nanosphere surface to approximately 7,000. Though that is not quite the number of PEG-SH molecules that demonstrated protection in Ch.chapter 3, the combination of the 7,000 PEG chains and the antibodies clearly protected the spheres from agglomeration. This is evidenced by the lack of radius increase when the fully labeled and protected nanospheres are diluted with an equal volume of commercial PBS solution, as shown in Figure 11. Since the radial growth of the spheres matched its predicted behavior fairly well, the decision was made to progress to useing the nanospheres to label a cell culture monolayer.

5 Results of the 6 March Labeling Session

With the PEGylation process fully optimized, we took the first step towards immunolabeling a full 3D artificial cornea, namely immunolabeling of a monolayer of cells on a microscope cover slip. The cells used were human dermal fibroblasts (HDFs) that express $\alpha 5\beta 1$-integrin, the same surface protein that we are targeting on the corneal cells. Performing immunolabeling on the monolayer allows assessment of the efficacy of the indirect immunolabeling process only, disregarding the collagen and removing the financial and temporal costs of building a complete corneal construct.

5.1 Structure of the Immunolabeling Experiment

Several different preparations were used to determine the efficacy of the immunolabeling process. Each of them removes one or more key components of the process, which should yield to very little increase in the scattering contrast. The 6 preparations(?) and their expected outcomes are described in the table below.

Preparation Name	1ary Ab?	2ary Labeler?	+Scattering Expected?	+Fluorescence Expected?
Cells Only	No	No	No	No
2 only	No	Secondary Ab	No	No
1–2	Yes	Secondary Ab	No	Yes
2Au	No	OPAb-Au-PS	No	No
1–2Au	Yes	OPAb-Au-PS	Yes	Yes
Au	No	Naked Au	See Below	No

Only those preparations with both primary and secondary antibodies should see an increase in the fluorescence signal, demonstrating the specificity of the secondary-to-primary binding. The 2 only and 1–2 samples were necessary to rule out any effects the Au nanospheres might have on the process. Scattering increase should only appear in the 1–2Au sample, because only the 1–2Au sample has both the gold to increase scattering and the secondary-primary binding to keep the gold bound to the cells. The one exception to this is the naked Au sample, where van der Waals forces and the presence of the salt solution may cause the spheres to agglomerate and stick to both the cells and the cover slip, causing a scattering increase.

The cells were prepared according to the procedure found in **??**; in brief, the procedure is

1. Fix cells with paraformaldehyde
2. Permeabilize with Triton-X
3. Label the nuclei with Sytox Green and the actin filaments with phalloidin (fluorescent stains)
4. Add primary if appropriate for a given preparation
5. Add appropriate secondary labeler

Each preparation had three different samples (except for 2Au, which had two) to minimize intrinsic variation during inter-preparation comparison. After labeling, each sample was imaged in three different places with the confocal microscope, using both fluorescence and

backscattering modes, and then each sample was imaged at five different $500\,\mu\text{m} \times 500\,\mu\text{m}$ field of view locations with the OCM (except for 2Au, for which each sample was sampled at 10 different locations).

5.2 Results of the Immunolabeling Experiment

Representative confocal images for each labeled sample are shown in Figure 14. Comparison between the 2 only and 1–2 confocal images reveals trails of green dots away from the nucleus only in the 1–2 sample; this is the expected pattern of labeled integrins. The appearance of stained integrins in only the 1–2 preparation indicates that both the primary and secondary antibodies bind only to the integrin and primary antibody, respectively. The samples with gold, however, are not as encouraging. Appearance of distinguishable cellular features in the back-reflectance channel indicates that the gold spheres bind to the cells–and to the cover slip–regardless of the presence of either the primary or secondary antibody. Nevertheless, cellular features are more easily distinguished in the 2Au samples, and most easily in the 1–2Au sample. This seems to indicate that some specific binding is occurring, but that a large amount of nonspecific binding is occurring as well.

Representative OCM images for the preparations labeled with gold as well as unlabeled cells are shown in Figure 15. Clearly, all three gold-labeled preparations show a significant increase in scattering compared to the unlabeled cells. However, as in the confocal images, the Au and 2Au preparations show a strong increase in scattering, and allow for cellular features to be distinguished. Also correlated with the confocal images is the ease with which cellular features can be distinguished: the images from the Au preparation all have a very strong homogenous background, making it harder to discern the features, and in general the cellular features of the 1–2Au more easily distinguishable than those of the 2Au.

To quantify the amount of scattering increase, the sum of squares of the values of each voxel was tabulated for each OCM image. The mean and standard error of all the images from a given preparation were then calculated; those results are shown in Figure 13. The increase in scattering in all three gold-labeled samples is shown quantitatively by comparing their sum of voxel values squared to that of the unlabeled cells. Among the gold-labeled samples themselves, the amount of scattering increase was the opposite of expected: the Au had the most scattering, then 2Au, then 1–2Au. However, the 2Au and 1–2Au samples are statistically indistinguishable.

The high amount of nonspecific binding was puzzling, and two hypotheses were put forth to explain the results of the labeling experiment. One possibility is that all of the spheres, especially the naked Au, bound to the cells via van der Waals forces. Because the naked Au has no dielectric separating it from whatever surface it comes in contact with, the strength of van der Waals forces will likely be much larger for the naked Au than for the 2Au. The second possibility concerns the use of Triton-X, a permeabilizing agent. Triton-X is used to permeabilize the cells so that the Sytox Green and phalloidin stains can diffuse inside the cell and stain the nucleus and actin cytoskeleton, respectively. Triton-X is a surfactant and permeablizes the cells by using surface tension to tear holes in the cell membrane. As a result, it was possible that the pores created by permeabilization of the cells allowed Au and 2Au to diffuse into the cell, but once in the cell, the gold nanospheres could not be removed by the washing process, leading to nonspecific contrast enhancement from nanoparticles inside the cell rather than on its surface. Furthermore, noting the strong background in some of the OCM images, there was some concern regarding the binding of the nanospheres to the coverslip surface itself. These concerns (van der Waals, permeabilization, and cover

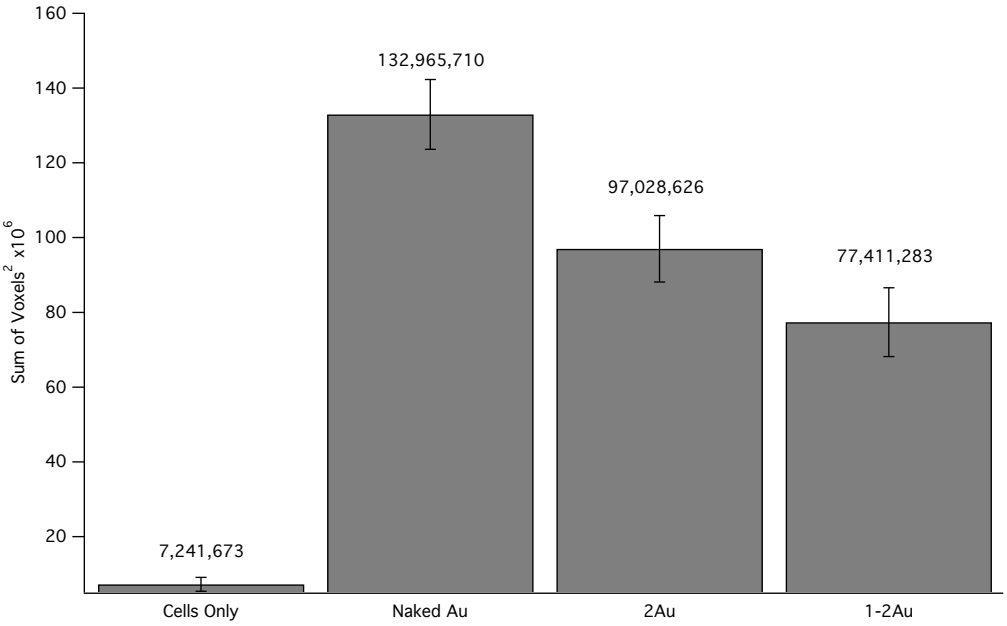

Figure 13: Sum of voxel values squared for gold-labeled preparations and unlabeled cells. Values are formed by taking the mean and standard error of sum of voxel values squared for each image corresponding to a given preparation.

slip binding) led to a second round of immunolabeling experiments being performed on 3 April.

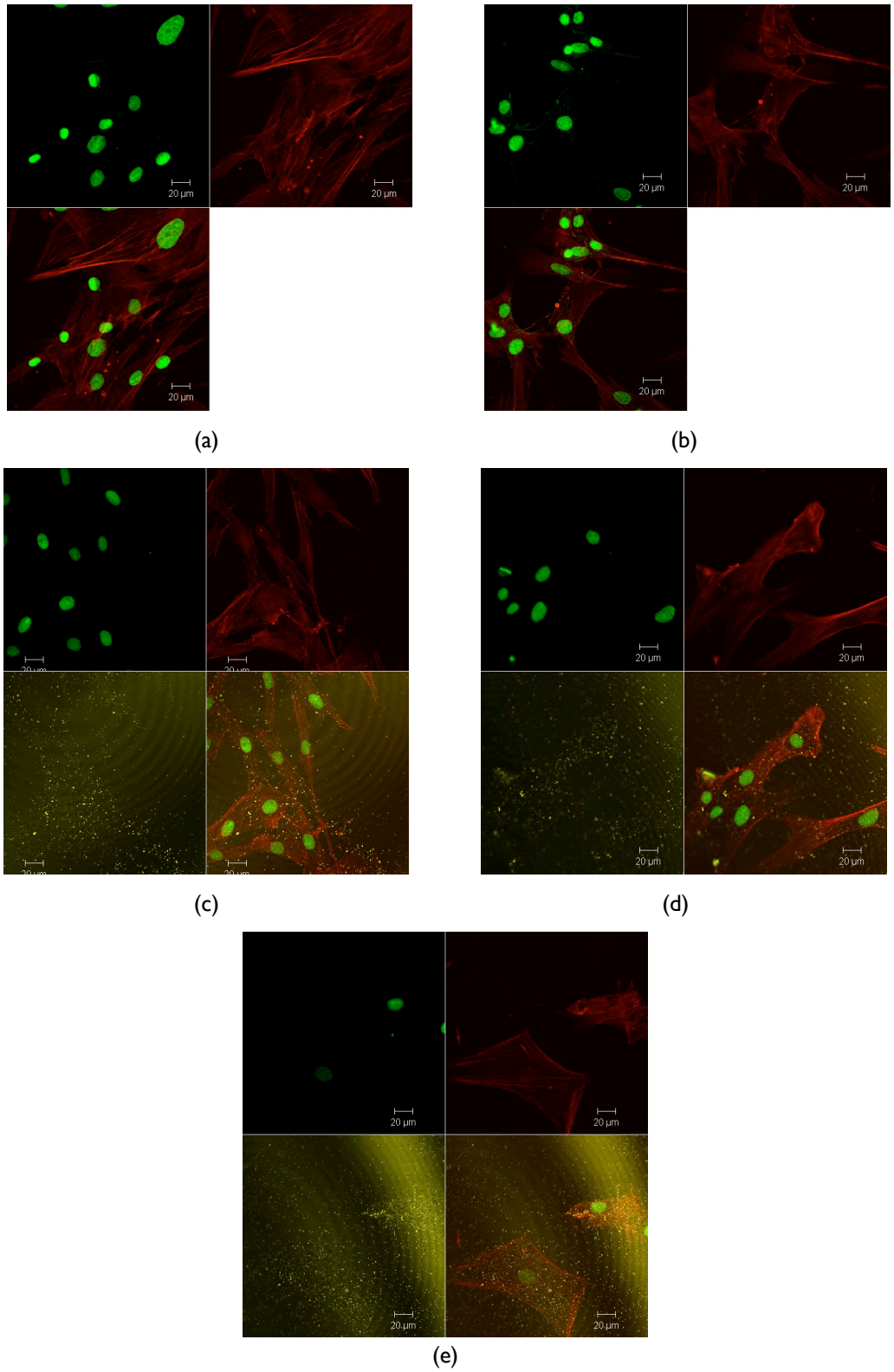

Figure 14: Confocal images of labeled preparations. Each image is a split view, showing Sytox and AP124F fluorescence (top left), phalloidin fluorescence (top right), backscattered light (c–e only; bottom left), and the composite view (bottom left, a and b; bottom right, c–e). Images correspond to preparations: (a) 2 only; (b) 1–2; (c) 1–2Au; (d) 2Au; (e) Au.

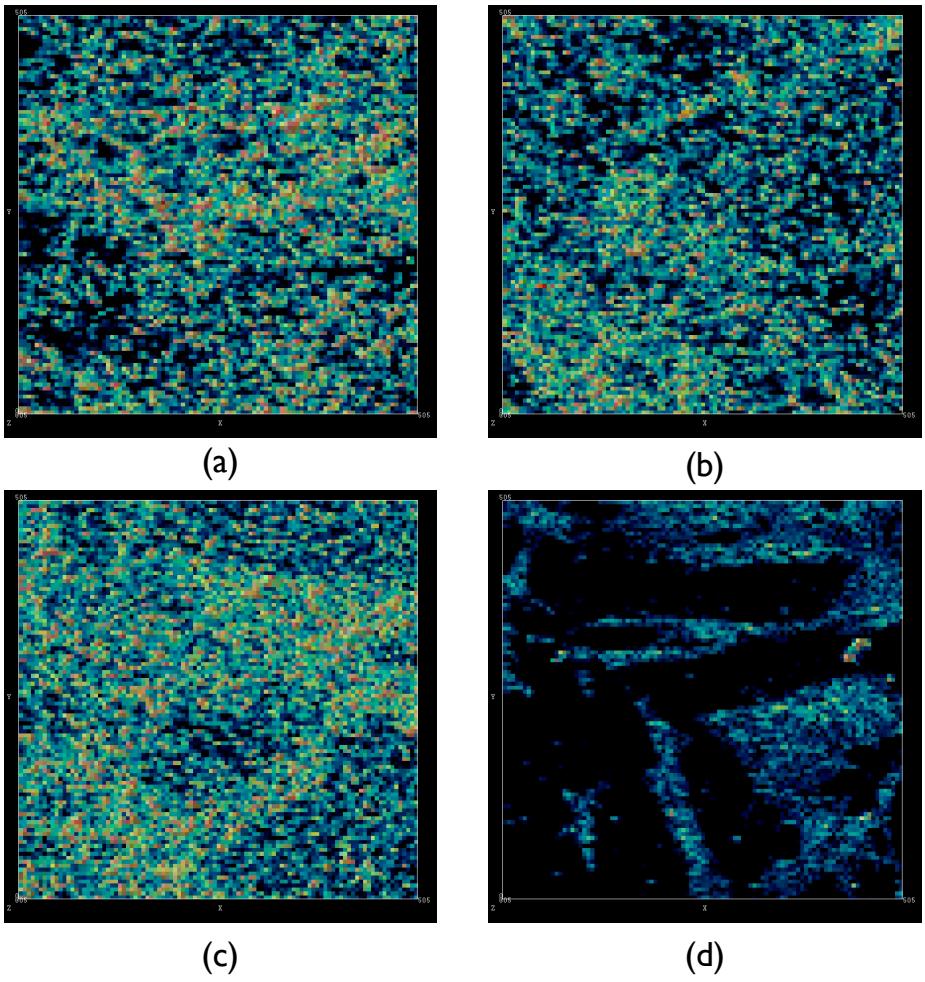

Figure 15: OCM images of labeled preparations. Images correspond to preparations: (a) 1–2Au; (b) 2Au; (c) Au; (d) Cells only.

6 Results of the 3 April Labeling Session

Bibliography

[1] Clarence W. C. Chan and Jamie L. Shoffeit. *Antibody-Gold Nanoparticle Conjugation for Immunogold Labeling in Optical Coherence Microscopy.* PhD thesis, Harvey Mudd College, May 2006. 3

[2] David Coats. *Visualization of Cells and Cell Phenotype in Tissue-Engineered Corneas via Immunogold Labeling.* PhD thesis, Harvey Mudd College, 2008. 5

[3] Perry Ellis and Oliver Hoidn. Pegylation of antibodies to gold nanospheres. August 2010. 5, 9, 14

[4] Hannes Fischer, Igor Polikarpov, and Aldo F. Craievich. Average protein density is a molecular-weight-dependent function. *Protein Science*, 13(10):2825–2828, 2004. 14

[5] National Eye Institute. Facts about the cornea and corneal disease. 3

[6] Inc. Laysan Bio. Hydrolysis half-lives. 7

[7] Amanda R Lowery, André M Gobin, Emily S Day, Naomi J Halas, and Jennifer L West. Immunonanoshells for targeted photothermal ablation of tumor cells. *International Journal of Nanomedicine*, 1(2):149–154, 2006. 4, 5, 9

[8] T Miron and M Wilchek. A spectrophotometric assay for soluble and immobilized n-hydroxysuccinimide esters. *Analytical Biochemistry*, 126(2):433–435, 1982. 7

[9] Pierce Protein Research Products. Chemistry of crosslinking. 7

[10] Chris B. Raub, Elizabeth J. Orwin, and Richard C. Haskell. Immunogold labeling to enhance contrast in optical coherence microscopy of tissue engineered corneal constructs. In *Proceedings of the 26th Annual International Conference of the IEEE, Engineering In Medicine and Biology Society*, volume 1, pages 1210–1213, 2004. 3

[11] Konstantin Sokolov, Michele Follen, Jesse Aaron, Ina Pavlova, Anais Malpica, Reuben Lotan, and Rebecca Richards-Kortum. Real-time vital optical imaging of precancer using anti-epidermal growth factor receptor antibodies conjugated to gold nanoparticles. *Cancer Research*, 63(9):1999–2004, 2003. 3

[12] Yih Horng Tan, Maozi Liu, Birte Nolting, Joan G. Go, Jacquelyn Gervay-Hague, and Gang-yu Liu. A nanoengineering approach for investigation and regulation of protein immobilization. *ACS Nano*, 2(11):2374–2384, 2008. 14, 15

[13] Robert Warren. *Immunogold Labeling of a Tissue-Engineered Cornea: Increasing the Binding Specificity of Immunogold Labeling via PEGylation.* PhD thesis, Harvey Mudd College, 2010. 4, 9